Combined use of physically based hydrological model and empirical models to improve parameterisation of erosion processes in a flash flood prone catchment

Atiyeh Hosseinzadeh, Hélène Roux, Ludovic Cassan, Audrey Douinot

Received: 15 November 2023 | Revised: 11 July 2024 | Accepted: 14 July 2024

DOI: 10.1002/esp.5946

RESEARCH ARTICLE

ESPL WILEY

Combined use of physically based hydrological model and empirical models to improve parameterisation of erosion processes in a flash flood prone catchment

Atiyeh Hosseinzadeh[1] | Hélène Roux[1] | Ludovic Cassan[1,2] | Audrey Douinot[1,3]

[1]Institut de Mécanique des Fluides de Toulouse (IMFT), Université de Toulouse, CNRS, Toulouse, France

[2]CECI, CERFACS/UMR5318 CNRS, Toulouse, France

[3]Écorce, Ingénierie & Consultance, Liège, Belgium

Correspondence
Hélène Roux, Institut de Mécanique des Fluides de Toulouse (IMFT), Université de Toulouse, CNRS, Toulouse, France.
Email: helene.roux@imft.fr

Present addresses
Ludovic Cassan, CECI, CERFACS/UMR5318 CNRS, Toulouse, France; and Audrey Douinot, Écorce, Ingénierie & Consultance, Liège, Belgium.

Funding information
Office Français de la Biodiversité; Région Occitanie Pyrénées-Méditerranée, Grant/Award Number: 20007302/ALDOCT-000988

Abstract

This study assesses the effectiveness of a distributed physically based hydrological model (MARINE) to investigate erosion estimation during flash floods compared with other widely used empirical models derived from the Universal Soil Loss Equation (USLE) like Revised Universal Soil Loss Equation (RUSLE) and Modified Universal Soil Loss Equation (MUSLE). It is carried out on a small catchment in south-eastern France, the Claduègne catchment. To compare the erosion volumes simulated by the three models, MARINE, MUSLE and RUSLE, a sensitivity analysis on the model parameters is carried out. According to physics-based simulations, flood events fall into two categories: those dominated by raindrop erosion and those dominated by shear stress erosion. The results show that the erosion simulated by the three methods are comparable, except for events dominated by raindrop erosion suggesting that further research is needed to improve raindrop erosion within MARINE. Simulations from the MARINE model provide access to the spatio-temporal variability of erosion dynamics during the event and can also be used to produce erosion/deposition maps, which are useful for environmental decision-makers and planners in identifying areas at risk from erosion and deposition hazards.

KEYWORDS
flash flood, MUSLE/RUSLE, physics-based hydrological model, soil erosion, suspended sediment transport, Universal Soil Loss Equation

1 | INTRODUCTION

Flash floods happen due to intense rainfall in a brief time span, typically lasting less than 6 h, in a limited geographical area and lead to rapidly increasing water levels (USGS by Kansas Water Science Center, 2005). Flash floods, which are widely recognized for their significant loss of life in densely populated areas, are frequently observed in the Mediterranean region (Kaffas et al., 2022). Flash floods also have the potential to cause severe soil erosion and significant sediment transport, leading to the permanent loss of soil from an area (Borga et al., 2014). Key factors associated with large flash floods include the intensity of the precipitation forcing and the hydrological behaviour of the catchment. Sediment transport is the process by which individual soil particles are separated from their original position and moved to different locations by various mechanisms using driving forces such as water or wind. Soil erosion is the general term used to describe the loss of soil, primarily from the surface. González-Hidalgo et al. (2007) stated that each year the three highest daily erosive events account for 50% of the total annual and inter-annual soil erosion in the Western Mediterranean area.

Understanding the process of soil erosion and sediment transport during flash floods is crucial as this could affect the geomorphology, hydrology and ecology of river systems (David et al., 2012; León et al., 2017; Sadaoui et al., 2016). Several studies conducted in mountainous areas have shown that extreme flood events lead to a significant increase in the morphological processes and could result in geomorphological changes in river channels (Bannari et al., 2016; Fortugno et al., 2017). These changes affect the hydraulic and

hydrological conditions of the channel and have implications for flood risk planning and management in the catchment.

Sediment transport presents significant risks to biodiversity and habitats, as it can lead to various detrimental effects. Consequently, it is crucial to assess erosion risks as part of a comprehensive biodiversity strategy. Stefanidis et al. (2022) conducted an assessment of soil erosion in specific areas of Crete Island to investigate its impact on biodiversity, habitat types and conservation practices. The results highlighted the importance of prioritizing soil erosion prevention as an integral part of biodiversity conservation efforts, particularly in areas of greater biodiversity.

Studying sediment transport during flash floods can gain insight into the complex nature of these events and contribute to better predictions. This knowledge can help to develop effective management strategies to reduce the adverse effects of flash floods, preserve river ecosystems and maintain the stability of sediment-related processes in river systems. Over the past few decades, numerous numerical models have been developed to improve the understanding of river behaviour in terms of sediment transport, from the distinction between suspended load and bed load models to physical and chemical transport models, classified as empirical, conceptual or process oriented (Aksoy & Kavvas, 2005; Papanicolaou et al., 2008). The aim was to predict soil erosion processes at different temporal and spatial scales since the inception of the early prediction equations in the 1940s (Borrelli et al., 2021).

A comprehensive review of soil erosion modelling from 1994 to 2017 was conducted by Borrelli et al. (2021) to identify the frequently addressed processes and models in the literature. Their database, named Global Applications of Soil Erosion Modelling Tracker (GASEMT), comprises 3030 individual records of soil erosion models from 126 countries, encompassing three categories: empirical, semi-empirical and physically based (or process oriented). A total of 435 different models and model variants are listed in the GASEMT database, but 25 of these are the most common. The empirical category is predominantly represented by USLE-type models, including Universal Soil Loss Equation (USLE) and Revised Universal Soil Loss Equation (RUSLE). In the semi-empirical category, models like Soil and Water Assessment Tool (SWAT) and Modified Universal Soil Loss Equation (MUSLE) are prominent. The remaining four models (MMF in Morgan et al., 1984; WEPP-Water Erosion Prediction Model in Laflen et al., 1991; LISEM-LImburg Soil Erosion Model in De Roo et al., 1996; and RHEM in Nearing et al., 2011) are either semi-physically based, which combines features of both physically based and empirical models, or physically based models. Overall, the research community is currently focused on enhancing the application of sophisticated process-oriented models while simultaneously updating existing empirical approaches like USLE, which continues to be practical and widely used. It is also evident that in many cases, the choice of soil erosion model is not driven by the need to accurately calculate erosion rates for a specific scenario, or by the desire to better understand both natural and anthropogenic soil erosion processes, but rather to obtain a risk assessment and to compare different soil conditions. These requirements contribute to the continued popularity of simple and time-efficient soil erosion models as the most commonly employed approaches. Nonetheless, there is a recognized need for a shift towards greater utilization of physically based models in the future. In the same spirit, Nguyen et al. (2016) discuss the hydrological models dedicated to flash floods and state that using hydraulic models shows a significant advantage in the capacity to simulate fluid flow. This allows them to accurately represent the flow dynamics with minimal parameters and could result in better prediction of sediment transport.

The motivation behind this study is to apply a simple and parsimonious model with physically meaningful parameters to estimate soil erosion and resulting suspended sediment transport during flash flood. By taking into account hydrological processes such as infiltration, overland flow and channel routing, the MARINE model (Modélisation de l'Anticipation du Ruissellement et des Inondations pour des évéNements Extrêmes in Roux et al., 2011) can accurately simulate flood events. Some examples of relevant simulations of the MARINE model can be found in Garambois et al. (2015a) for regionalisation purposes or in Eeckman et al. (2021) for soil saturation modelling. According to Cea et al. (2016), this type of hydrodynamic model, which is physically based, parsimonious and allows estimation of uncertainty, should be encouraged for soil erosion studies. Soil erosion and the resulting sediment transport estimated by the spatially distributed hydrological model MARINE are compared with widely used empirical models, MUSLE and RUSLE, to help answer the following question: how the combined use of the physically based hydrological model MARINE and the empirical models MUSLE and RUSLE can help to achieve consistency and physical meaning in the parameters of the empirical models at the catchment scale and improve the simulation of erosion processes?

The paper structure is as follows: Section 2 describes the modelling approach: study site, model implementation and intercomparison method. Section 3 presents the results that are discussed in Section 4 to identify the strengths and limitations of each type of model, and finally, concluded in Section 5.

2 | METHODOLOGY AND METHODS

This section is organized as follows: Section 2.1 describes the study site. MARINE model and its data requirements are presented in Section 2.2, MARINE implementation and sensitivity analysis (SA) approach used to calibrate both the hydrodynamic and suspended sediment transport modules in Section 2.3, RUSLE and MUSLE model descriptions and their implementations in Section 2.4, Section 2.5 and Section 2.6. Model intercomparison methodology is described in Section 2.7.

2.1 | Study site

The study site is the Claduègne (Figure 1), a 42.3 km^2 research catchment, in the Cévennes-Vivarais Mediterranean Hydrometeorological Observatory (OHMCV Observatory—Ozcar-Ri, n.d.). The region experiences an oceanic and Mediterranean climate, with heavy rainfall and flash floods during autumn (Uber, 2020). The annual precipitation in the catchment ranges from 850 to 900 mm (Nord et al., 2017). Autumn has the highest monthly precipitation, followed by a secondary peak in spring. In general, the maximum sediment transport occurs during the autumn season (Uber, 2020). The Claduègne catchment exhibits two distinct geological features. The southern part consists of

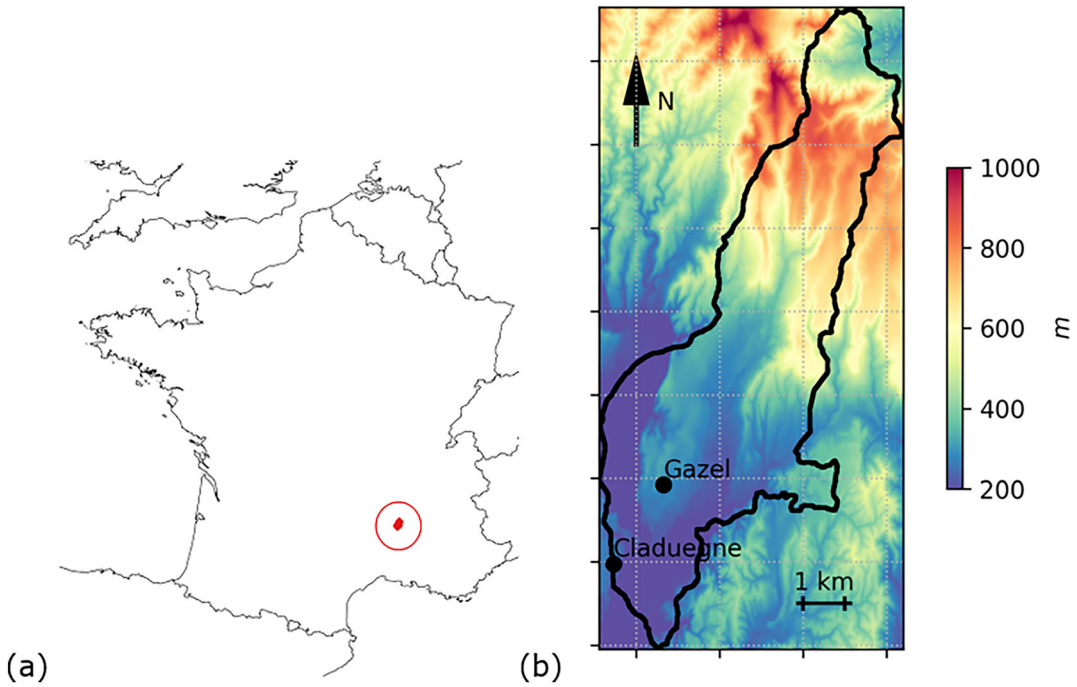

FIGURE 1 Study area: (a) geographic location of the Claduègne catchment and (b) 1 m DEM created from an aerial LiDAR dataset acquired in 2012 and processed by Sintégra (Braud et al., 2014), provided by Nord et al. (2017), with two gaging stations: Claduègne (outlet) and Gazel (Hosseinzadeh et al., 2022).

piedmont hills with sedimentary limestone rocks beneath, while the northern area comprises the Coiron basaltic plateau, bordered by sheer cliffs of basaltic columns (Nord et al., 2017). Nord et al. (2017) state that the main land-use types in the area include pastures, vineyards and forests. The land cover map shows that forests and shrublands occupy the largest area, accounting for 61% of the watershed, followed by vineyards (16%) and an equal share of grasslands and cultivated fields (11% each).

Digital elevation model (DEM), soil properties, vegetation or land-use and rainfall as well as continuous observations of discharge for the Claduègne catchment are obtained from Nord et al. (2017). In the catchment area, a research network named Hpiconet[1] includes 21 rain gauges that collect rainfall data at 5 min intervals. The catchment also has two additional rain gauges, Berzème and Vogüé, which are managed by the French flood forecasting service SPC Grand Delta and operate with a resolution of 5 min. The water depth in the river is assessed using an H-radar sensor at a 10-min interval for the Claduègne gaging station (Figure 1). The discharge is estimated from the water level data using a stage-discharge relationship established through the BaRatin framework (Le Coz et al., 2014; Uber, 2020). Suspended sediment concentration (SSC) is estimated using a turbidity–SSC rating curve as discussed by Uber (2020) using continuous turbidity data which are provided by the Hydrology Observatory DataBase (BDOH) (Branger & Thollet, 2016). The initial soil saturation is derived from Météo-France's SIM operational chain (Habets et al., 2008) which provides the ratio between soil water content and storage capacity, at a resolution of 8 km × 8 km.

Based on Braud et al. (2014), flash floods refer to rapid flood events with a hydrograph rise happening in a few hours for catchments smaller than 100 km^2 and within 24 h for catchments larger than 1000 km^2. To identify flash floods in our catchments, we used an arbitrary threshold of 0.1 $m^3/s/km^2$ for specific peak discharge. This is slightly lower than the threshold of 0.5 $m^3/s/km^2$ proposed by Gaume et al. (2009) and Braud et al. (2014) for identifying flash floods, but it allows us to have a sufficient sample of events while considering only the most extreme ones. The beginning and the end of each event is arbitrarily defined as 2 days before and 1 day after the discharge peak but further studies should consider a more relevant way based on both rainfall and discharge signals, such as Huynh et al. (2023). The characteristics of the selected events according to the available observations are shown in Table 1.

2.2 | MARINE model description

The MARINE model is a distributed and mechanistic hydrological model specifically designed for simulating flash floods (Roux et al., 2011) and including a suspended sediment transport model (Hosseinzadeh et al., 2022). As detailed in Roux et al. (2011), it includes three main hydrodynamic modules: infiltration, subsurface flow and surface flow representing both overland and channel flows. The transfer function component, based on an approximation of the Saint-Venant equations, transports the rainfall excess to the catchment outlet. The catchment is spatially discretized using a regular grid of square cells based on the DEM grid resolution. The spatial resolution of this grid is 100 m × 100 m in the Claduègne catchment.

One of the significant advantages of the MARINE model is its ability to utilize spatial information through distributed input data, such as catchment spatial properties and rainfall. It calculates the water balance for each cell in every time step, considering its location in either the hillslope or the drainage network. Additionally, the model

[1] http://www.ohmcv.fr/hpiconet/index.html, last access: 10 May 2023.

TABLE 1 Characteristics of the studied flood events: peak discharge (Q_{peak}, m^3/s), peak suspended sediment concentration (SSC_{peak}, g/L), averaged cumulative rainfall depths over the catchment area (mm) and maximum local precipitation intensity during the event (mm/h).

Flood event	Q_{peak} (m^3/s)	SSC_{peak} (g/L)	Cumulated rainfall (mm)	Max. intensity (mm/h)
2011/11/04	28.4	11.6	144.4	72
2013/05/18	84.0	17.7	59.6	49
2013/10/20	54.6	11.5	89.1	82
2014/01/04	63.6	4.1	72.1	24
2014/01/19	104.0	6.8	114.9	18
2014/02/05	29.4	2.3	29.3	13
2014/09/19	91.6	17.2	101.8	168
2014/10/10	48.3	3.7	77.2	52
2014/10/13	35.9	3.2	30.8	97
2014/11/04	212.5	31.1	222.1	60

can simulate the flood hydrograph at any location in the drainage network and monitor changes in distributed variables like soil moisture and overland flow velocities throughout the catchment (Roux et al., 2011).

MARINE uses the depth-averaged scalar mass conservation equation to simulate the spatio-temporal evolution of the SSC for non-cohesive sediments, incorporating source terms to represent erosion and deposition (Equation 1).

$$\frac{\partial(hc)}{\partial t}+\frac{\partial(hUc)}{\partial x}=E_r+D_r, \tag{1}$$

where h is water depth (m), c is SSC in volume fraction (m^3/m^3), U is velocity (m/s), E_r is net flux of shear stress eroded sediments (m/s) and D_r is raindrop erosion rate (m/s).

E_r (m/s) is determined using the concentration at equilibrium model proposed by van Rijn (1984) (Equation 2).

$$E_r=w_c(c_{eq}-c_{ref}) \tag{2}$$

c_{eq} and c_{ref} (-) are the concentration at near-bed equilibrium and reference concentration, respectively. The fall velocity w_c (m/s) follows van Rijn (1984) formula (Equation 3):

$$w_c=\begin{cases}\left(\frac{\rho_s}{\rho}-1\right)\frac{g{d_{50}}^2}{18\upsilon} & \text{for } d_{50}<10^{-4}m,\\ \frac{10\upsilon}{d_{50}}\left(\left(1+0.01\left(\frac{\rho_s}{\rho}-1\right)\frac{g{d_{50}}^3}{\upsilon^2}\right)^{0.5}-1\right) & \text{for } 10^{-4}<d_{50}<10^{-3}m,\\ 1.1\left(\left(\frac{\rho_s}{\rho}-1\right)gd_{50}\right)^{0.5} & \text{for } d_{50}\geq 10^{-3}m.\end{cases} \tag{3}$$

υ is kinematic viscosity (m^2/s), d_{50} represents the median diameter of sediment particles (m), ρ_s is the particle density (kg/m^3), ρ is the fluid density (kg/m^3) and g is the gravitational acceleration (m/s^2).

The concentration at near-bed equilibrium c_{eq} (-) is calculated at a specific height above the bed, denoted as z_{ref} (m) (Equation 4, in van Rijn, 1984). This height is determined as the interface between bed load and suspended load.

$$c_{eq}=0.015\frac{d_{50}}{z_{ref}D_*^{0.3}}\left(\frac{\tau_p}{\tau_c}-1\right)^{1.5}. \tag{4}$$

τ_p (kg/ms^2) is the bed shear stress calculated using Equation (5) where FSE (-) is the coefficient of sensitivity of the soil to shear erosion, that is, the ratio between effective (τ_p) and total shear.

$$FSE=\frac{\tau_p}{\rho g h S_h}, \tag{5}$$

with S_h (m/m) the topographical slope. τ_c (kg/ms^2) refers to the critical shear stress required for initial movement of sediment particles through erosion. It can be calculated as a function of the dimensionless diameter D_* (Equation 6, in Tassi & Villaret, 2014).

$$D_*=\left[d_{50}\left(\frac{\rho_s}{\rho}-1\right)\frac{g}{\upsilon^2}\right]^{1/3}. \tag{6}$$

In the context of steady uniform flow, integrating the Rouse equation on the vertical allows to write a relationship between the reference concentration c_{ref} and the depth average concentration $\bar{c}$ (Viollet et al., 2003) (Equation 7).

$$c_{ref}=\begin{cases}\frac{(1-R_o)(h-z_{ref})}{{z_{ref}}^{R_o}\left(h^{1-R_o}-{z_{ref}}^{1-R_o}\right)}\bar{c} & \text{if } R_o\neq 1,\\ \frac{(h-z_{ref})^2}{z_{ref}\left(-h\times ln\left(\frac{z_{ref}}{h}\right)-h+z_{ref}\right)}\bar{c} & \text{if } R_o=1,\end{cases} \tag{7}$$

where R_o (-) is the Rouse number (Equation 8).

$$R_o=\frac{w_c}{\kappa\sqrt{ghS_h}}. \tag{8}$$

κ (-) is von Karman constant (standard value of 0.41).

The raindrop erosion rate D_r (m/s) is that proposed by Wicks and Bathurst (1996) (Equation 9).

$$D_r=\frac{k_r}{\rho_s}F_w KE. \tag{9}$$

k_r (kg/m^2/s^2) is an erodibility coefficient. It was estimated from four experimental data and describes the ease of detachment by a raindrop, so qualitatively, it is expected to increase from clay, through silt, to sandy soil (Table 2).

F_w (-) is a water depth correction factor: It decreases exponentially with increasing water level h (Equation 10, in Wicks & Bathurst, 1996).

$$F_w = \begin{cases} \exp\left(1 - \frac{h}{d_{rain}}\right) \text{ if } h > d_{rain}, \\ 1 \text{ otherwise.} \end{cases} \quad (10)$$

The raindrop diameter d_{rain} (m) is calculated based on the rainfall intensity I_{rain} (mm/h) (Equation 11, in Laws & Parsons, 1943).

$$d_{rain} = 0.00124 I_{rain}^{0.182}. \quad (11)$$

KE (kg^2/s^3) is the kinematic energy of precipitation (Wicks & Bathurst, 1996). A non-linear relationship is assumed between KE and rainfall intensity I_{rain} (Equation 12).

$$KE = a_r I_{rain}^{b_r}. \quad (12)$$

a_r and b_r are empirical coefficients that vary with rainfall intensity. Corresponding values can be found in Wicks and Bathurst (1996).

2.3 | MARINE implementation

The use of physically based models is hampered by problems of overparameterization and equifinality, making it difficult to identify parameter values during calibration (Beven, 1989). To address this, SA is used to identify critical parameters and improve the model structure (Sieber & Uhlenbrook, 2005).

The calibration process for the hydrodynamic module is explained in detail by Roux et al. (2011) and Garambois et al. (2015b). This involves conducting SA to investigate the impact of each model parameter on the simulated output and to select suitable calibration events. The hydrological part of the MARINE model has been calibrated on the catchment at a spatial resolution of 100 m × 100 m, as part of a previous unpublished study on both Cladueègne and Gazel stations (Figure 1) using the six following events (Table 1): 4 November 2011, 18 May 2013, 20 October 2013, 4 January 2014, 13 October 2014 and 4 November 2014. Calibration was carried out by optimizing the NASH criterion between observed and simulated discharges for the six events at the two gauging stations with respect to five tunable parameters regulating the volume of water passing through the subsurface and the dynamics of surface run-off. The reader is referred to Garambois et al. (2015b) for further information on the calibration procedure. The value of the calibrated parameters for the hydrodynamic module is presented in Table 3.

The hydrological calibration is not event based, but it is an averaged calibration for the catchment as explained in Garambois et al. (2015b). As will be explained later (Section 3.1 and Table 6), this results in a more robust calibration with overall better prediction capabilities, but the performance on each event is obviously less satisfactory than an event-specific calibration. However, event-specific calibration is useless for forecasting, so the average calibration is maintained, even if the event performance is sometimes less satisfactory.

A similar methodology is applied to the suspended sediment transport module. As it has been discussed in Section 2.2, the suspended sediment transport model relies on several key parameters to calculate the net sediment flux, which include:

- d_{50} (m) the median diameter of sediment particles,
- z_{ref} (m) the location of the interface between bed load and suspended load,
- FSE (-) the coefficient of soil sensitivity to shear erosion, determined by the ratio of effective shear stress to total shear stress (Equation 5) and
- k_r (kg/m^2/s^2) the coefficient of soil sensitivity to raindrop erosion (Equation 9).

The ranges of variation for these parameters are predetermined based on their physical significance and insights from previous studies like Wicks and Bathurst (1996) and Uber (2020) (Table 4). Monte Carlo simulations are then performed by running the model with various randomly selected sets of parameter values. Each set is assigned a likelihood of accurately simulating the system, based on the chosen likelihood measure. The results of this previous SA are presented in Hosseinzadeh et al. (2022). They mainly show that the most sensitive

TABLE 3 Calibrated parameters of the hydrodynamic model for Cladueègne.

Parameter	Description	Value
C_Z (-)	Correction coefficient of the soil thickness	0.685
C_K (-)	Correction coefficient of the hydraulic conductivity	15.1
C_{Kss} (-)	Correction coefficient of the soil lateral transmissivity	1145.0
K_1 (m$^{1/3}$/s)	Strickler roughness coefficient of the main channel	11.2
K_2 (m$^{1/3}$/s)	Strickler roughness coefficient of the overbank	18.2

TABLE 2 Mean k_r (kg/m^2/s^2) coefficients for various soil textures from four experimental data (Wicks & Bathurst, 1996).

Soil texture	Clay	Silty clay	Silty loam	Silt	Silty clay loam	Loam	Sandy loam	Sand
k_r	19	18.2	16.2	29.8	39.8	28.2	32	30
						30		
	73.5		22.2		25.7	37.6	34.4	62.4
					24.7	23.4	30	

TABLE 4 Range of variation for the sensitivity analysis of the sediment transport parameters of the MARINE model.

Parameter	Min	Max	Sampling
d_{50} (mm)	0.010	0.150	Uniform
z_{ref} (m)	0.001	0.020	Uniform
FSE (-)	0.01	1.00	Uniform
k_r (kg/m^2/s^2)	0.0	100.0	Uniform

parameters are the coefficient of soil sensitivity to shear erosion, *FSE*, and the median diameter of sediment particles, d_{50}. Here, the parameter values providing the most satisfactory simulation on the basis of the chosen likelihood for each event are used for simulations and intercomparison with the RUSLE and MUSLE models.

The chosen error criterion NASH-S is the NASH calculated between simulated SSC and SSC estimated from continuous turbidity measurements and turbidity–SSC rating curve at the outlet (Claduègne gaging station of Figure 1). The parameters corresponding to the highest NASH-S help us draw trends and identify similarities between events. Moreover, analysing the variations in each parameter for the best SSC simulation of all events is helpful in assessing their consistency with the catchment characteristics.

To evaluate the performances of both hydrodynamic and sediment transport calculation, a second criterion L_{NP} has also been calculated, which includes peak characteristics (Roux et al., 2011), independent of the simulation window (Equation 13).

$$L_{NP} = \frac{1}{3}NASH + \frac{1}{3}\left(1 - \frac{\left|y_p^s - y_p^o\right|}{y_p^o}\right) + \frac{1}{3}\left(1 - \frac{\left|T_p^s - T_p^o\right|}{T_c}\right), \quad (13)$$

where y_p^s and y_p^o are, respectively, the simulated and observed peak (of discharge [m^3/s] for the hydrodynamic simulation evaluation and of concentration [g/L] for the SSC simulation evaluation); T_p^s and T_p^o are, respectively, the date of the simulated and observed peak; and T_c is the time of concentration in the catchment (h), assumed to be the same for water and sediment. According to Uber (2020), the time of concentration is estimated to be $T_c = 4.7$ h in the Claduègne catchment.

2.4 | Description of common factors of USLE-type model

USLE (Equation 14) was initially developed for agricultural plots in the United States of America to quantify soil loss (Wischmeier & Smith, 1978).

$$A = R \times K \times LS \times C \times P, \quad (14)$$

where A is soil loss (t/ha), R is the rainfall erosivity factor (MJ.mm/ha/h), K is the soil erodibility factor (t.h/MJ/mm), L and S are the topographical factors (-), C is the vegetation cover factor (-) and P is the soil conservation practice factor (-).

The R factor, K factor and LS factor have been subjects of extensive investigations in various studies. Alewell et al. (2019) assessed nearly 2000 publications related to soil erosion by water with particular emphasis on USLE type. They addressed recent advancements in individual USLE parameters and their significance in estimating soil loss results in RUSLE.

The proposed exponential relationship by Kinnell et al. (2018) for estimating the unit rainfall energy (e_r, MJ/ha/mm) based on rainfall intensity (i_r, mm/h) is given in Equation (15).

$$e_r = 0.29 \times [1 - 0.72\exp(-0.05 i_r)]. \quad (15)$$

The R factor (MJ.mm/ha/h) for each rainfall event, or rainfall erosivity, is determined by multiplying the total rainfall energy (E_{rain}) by the maximum 30-min intensity (I_{30}) of that rainfall event (Equation 16).

$$R_{\mathrm{RUSLE}} = E_{rain} I_{30} \text{ with } E_{rain} = \left(\sum_{r=1}^{k} e_r V_r\right), \quad (16)$$

with V_r the rainfall volume (mm) during the time interval, which in our case is the total duration of the event or simulation window, and I_{30} is the maximum 30-min rainfall intensity (mm/h). Dunkerley (2019) proposes to calculate the rainfall erosivity factor R_{RUSLE} using the maximum intensity for the entire event rather than the maximum intensity for 30 min in Equation (16). In fact, according to Dunkerley (2019), the 30-min I_{30} interval often does not capture the most intense rainfall periods, which typically account for a very small fraction of the total event duration, often less than 1%.

Initially, the soil erodibility or K factor was derived empirically, based on a dataset gathering over 20 years of observations on experimental plots featuring 23 major soil types across the United States (Alewell et al., 2019). Renard et al. (1997) proposed an estimation method for K factor (t.h/MJ/mm) based on geometric mean diameter of soil particles (D_g, mm) in SI unit (Equation 17).

$$K = 0.0034 + 0.045\, exp\left(-0.5((\log D_g + 1.659)/0.7101)^2\right). \quad (17)$$

The effects of topography are taken into account by two factors: slope length (L) and slope steepness factor (S), both dimensionless. Desmet and Govers (1996) proposed a formulation for L based on the upslope contributing area of each grid cell. For DEM grid based, the equation can be written as follows (Equation 18):

$$L_{i,j} = \frac{\left(U_{i,j} + D_{i,j}^2\right)^{m+1} - U_{i,j}^{m+1}}{D_{i,j}^{m+2} X_{i,j}^m (22.13)^m}. \quad (18)$$

The $U_{i,j}$ (m^2) is the area contributing to flow into the cell with coordinates (i,j). $D_{i,j}$ (m) is the grid cell size. The value of $X_{i,j}$ (-) depends on the flow direction relative to grid cell orientation $\alpha_{i,j}$ (Equation 19), and the product $D_{i,j}X_{i,j}$ (m) gives the effective length of the contour over which the discharge is flowing. The slope-length exponent m in Equation (18) is related to the ratio β of rill erosion (caused by shear stress) to inter-rill erosion (mainly caused by raindrops), which ranges from 0 to 1, following Equations (20) and (21) based on Renard et al. (1997), where θ is the slope angle in degrees.

$$X_{i,j} = \sin\alpha_{i,j} + \cos\alpha_{i,j}, \tag{19}$$

$$m = \frac{\beta}{1+\beta}, \tag{20}$$

$$\beta = \frac{(\sin\theta)/0.0896}{3(\sin\theta)^{0.8}+0.56}. \tag{21}$$

The *S* factor is often estimated using the empirical function suggested by McCool et al. (1987) based on the slope gradient (Equation 18).

$$S = \begin{cases} 10.8\sin\theta + 0.03 \text{ if } slope < 9\%, \\ 16.8\sin\theta - 0.5 \text{ if } slope \geq 9\%. \end{cases} \tag{22}$$

slope is measured in per cent. This study uses the slope at each grid cell calculated from the DEM. This *S* equation is suitable for regions characterized by minimal summer rainfall according to Schmidt et al. (2019). The validity of the various empirical *S* factors is limited to slope gradients below 100% (Alewell et al., 2019).

The cover-management factor or *C* factor (-) illustrates the influence of various cover and management practices that affect soil erosion (Wischmeier & Smith, 1978). Estimating the *C* factor is not easy due to the complexity of management practices and the difficulty of obtaining information on them in practice, limited data availability and challenges in processing all components on a large scale (Alewell et al., 2019). Panagos et al. (2015) determine the *C* factor for each CORINE Land Cover class based on literature from various countries in Europe, including France. Due to the variability of values found in the literature, a range of values was assigned to each class (Table 5).

The practice *P* factor is a dimensionless parameter that accounts for the effect of erosion control measures and farming practices on soil loss. When erosion control measures are not implemented, typical values range from around 0.2 for reverse-slope bench terraces to 1.0 (Alewell et al., 2019).

2.5 | Parameter estimation for USLE-type models

On the Claduègne catchment, the *K* factor is set to 0.03 t.h/MJ/mm using average value of the *K* obtained using the d_{50} of the best MARINE simulations for each flash flood events as the geometric mean diameter of soil particles D_g involved in Equation (17).

LS factor (-) is calculated using slope and flow accumulation driven by DEM at 100 m × 100 m resolution (Equations 18–22). The highest value of *LS* is found in the middle part of the catchment and on the hillslopes where the slope is high. Low elevation areas in the downstream part of the catchment results in low *LS* value. These findings are consistent with the outcomes reported by many other authors (Djoukbala et al., 2019). The *P* factor is assumed to be 1.0 considering no erosion control measures are applied in the catchment. The rainfall erosivity factor R_{RUSLE} is calculated using the maximum intensity for the whole event according to Dunkerley (2019). This maximum intensity is calculated using the rainfall data from rain gauges with a resolution of 5 min over a time window of 2 days before and 1 day after the peak flow rate.

TABLE 5 Range of cover-management *C* factor values for land cover in the Claduègne catchment according to Panagos et al. (2015).

Land cover type	Min *C*	Max *C*
Forests and shrublands	0.0001	0.003
Vineyards	0.15	0.45
Grassland	0.01	0.08
Cultivated fields	0.07	0.2

2.6 | Factors specific to the MUSLE model

MUSLE is based on the same Equation (14) as USLE, taking into account the same factors: erosivity (*R*), soil erodibility (*K*), topographical factors (*LS*), vegetation cover (*C*) and soil conservation practices (*P*). Williams (1975) demonstrated that substituting a run-off erosivity factor *R* instead of a rainfall erosivity factor in (R)USLE allowed for the estimation of sediment supply to stream networks during storm events. Williams (1975) introduced the MUSLE as an event-based erosion model to simulate soil erosion caused by surface run-off during flood events. The run-off erosivity factor *R* (MJ.mm/ha/h) for MUSLE model is represented by Equation (23).

$$R_{\text{MUSLE}} = a(VQ_p)^b, \tag{23}$$

where *V* is the volume of run-off (m^3), Q_p is the peak flow rate (m^3/s) and *a* and *b* are location-specific coefficients. In many catchment-scale applications, calibration data for the coefficients *a* and *b* are scarce, leading to the assumption of fixed values: $a = 11.8$ and $b = 0.56$, for metric system units (Sadeghi et al., 2014). All the other parameters in Equation (14) are the same as for the (R)USLE model (see Section 2.4).

Numerous studies lack consistent units for the parameters, particularly *R* and *K* (Gwapedza et al., 2018). According to Gwapedza et al. (2018), some authors have used Mg/MJ/mm for *K* units, while other used t.h/MJ/mm. In this study, our choice of the unit t.h/MJ/mm for the *K* factor ensures consistency with the units used for *R* in RUSLE and MUSLE, where *R* is in MJ.mm/ha/h and results in an estimate of erosion in t/ha.

In this study, the run-off erosivity factor R_{MUSLE} is calculated using the peak discharges and run-off volumes simulated by the MARINE model. These MARINE results are based on the SSC simulation with the highest NASH-S value calculated from sediment concentration among the Monte Carlo simulations in the SA of the sediment transport module.

2.7 | Methodology for model intercomparison

SSC estimations using MARINE model for each event are derived from the best simulations of the SA as explained in Section 2.3. Then, to compare the three models using the MARINE results as a reference, a SA is performed on the *C* value for MUSLE and RUSLE through each event. This analysis includes generating random uniform values ranging from a minimum of $C = 0.00001$ to a maximum of $C = 0.1$. The range is consistent with Panagos et al. (2015) in which

the *C* factor was defined for each CORINE Land Cover class as explain in Section 2.4 and Table 5. This study uses a sample of 5000 random *C* values, constants over the catchment. The purpose of this analysis is to estimate the *C* value within this range that led to the lowest root mean square error (RMSE) between erosion volumes (t/ha) simulated by MUSLE/RUSLE and MARINE (Equation 24).

$$\mathrm{RMSE} = \sqrt{\frac{1}{n}\sum_{i=1}^{n}\left(E_{\mathrm{MARINE},i} - E_{\mathrm{MUSLE/RUSLE},i}\right)^2}, \tag{24}$$

where *E* is erosion volume in t/ha, *i* is the number of the current cell and *n* is the total number of cells over the catchment.

The value of *C* is estimated on the basis of the eroded volumes simulated by MARINE, as the MARINE simulations are calibrated on the basis of turbidity measurements and turbidity–SSC rating curve at the outlet. However, this does not guarantee the quality of these simulations and in particular the spatial variability of the simulated eroded volumes. The questions behind this comparison are: Is it possible to find a value of the *C* factor that reproduces the erosion volumes estimated by MARINE? And if so, is this value of the *C* factor compatible with what we know about the actual land cover of the Claduègne catchment? Answering these questions will help us to identify the potential strengths/weaknesses of the three models on the basis of the *C* values obtained and the analysis of the best MARINE simulations carried out in Section 3.1.

In all three models, the coefficients *FSE*, k_r, *C* and *K* are assumed to be uniform across the entire catchment. Of course, soil sensitivity to erosion is in fact spatially variable, as explained for Claduègne in Uber et al. (2021). The choice to consider only uniform parameters certainly has an impact on the values estimated for these parameters, but it is made for two reasons. On the one hand, avoiding the complexity of the spatial variability of *FSE* and k_r makes it easier to interpret their influence on the MARINE model simulations. On the other hand, it facilitates intercomparison with the RUSLE and USLE models, which were originally designed to be applied globally over the entire catchment. Minimizing the RMSE helps identify the *C* values for RUSLE and MUSLE that results in simulations with similar erosion volumes for the three models at the catchment scale. By aiming to simulate similar erosion volumes between MARINE and MUSLE/RUSLE, we can gain insights into the differences in simulated behaviour between these models and their potential weaknesses and benefits.

3 | RESULTS

In the following, Section 3.1 analyses the results of the SSC simulated with MARINE model. Section 3.2 detail the model intercomparison.

3.1 | Analysis of SSC simulations using MARINE model

The value of each parameter in SA that results in the highest NASH-S score is considered as the best simulation (Table 6). When comparing the two columns of *FSE* and k_r, it becomes apparent that when one of them is low, the other tends to be high. Events may therefore be categorized as either *FSE* dominant or k_r dominant or rather shear stress erosion dominant or raindrop erosion dominant when considering the physical processes. Thus, four events (5 February 2014, 19 September 2014, 10 October 2014 and 13 October 2014) are categorized in k_r category and the remaining six events (4 November 2011, 18 May 2013, 20 October 2013, 4 January 2014, 19 January 2014 and 4 November 2014) in *FSE* category. The k_r category events, 5 February 2014, 10 October 2014 and 13 October 2014, typically have the lowest observed SSC and discharge (Table 1). However, this is not the case for k_r category event 19 September 2014, which has a lower NASH-H and will be analysed in more detail later. For these events, the simulated dominant mechanism of sediment production is the raindrop erosion, possibly related to the low shear stress and the rapid SSC response to rainfall in sedigraph. This is how the model simulates erosion and sediment transport during these events. In fact, once there is a sufficient depth of water due to run-off on the soil surface, the water protects the soil and raindrop erosion becomes negligible (Equation 10). This means that for the k_r-dominant events, the overland flow is low enough for this type of erosion to be simulated. However, there is no in situ observation to confirm this analysis of the simulated processes.

To assess the impact of k_r, simulations of the k_r-dominant events are run keeping the values of the other parameters but setting

TABLE 6 Parameter value for the best simulation in sensitivity analysis for each event with highest values highlighted in bold.

Event	d_{50} (10^5 m)	z_{ref} (mm)	*FSE* (-)	k_r (kg/m^2/s^2)	NASH-H	NASH-S	L_{NP}-H	L_{NP}-S
2011/11/04	3.2	6	0.11	0.01	<0	0.47	<0	**0.57**
2013/05/18	2.7	**17**	**0.24**	2.13	**0.56**	**0.89**	**0.60**	**0.82**
2013/10/20	3.3	2	0.04	0.52	0.08	**0.84**	0.50	**0.83**
2014/01/04	3.3	8	0.11	2.21	**0.69**	**0.86**	**0.66**	**0.83**
2014/01/19	3.8	**17**	**0.24**	1.67	**0.75**	**0.95**	**0.77**	**0.92**
2014/02/05	**11.0**	**16**	0.02	**61.52**	**0.63**	0.42	**0.64**	**0.54**
2014/09/19	1.2	10	0.01	**70.86**	0.26	**0.69**	**0.63**	**0.70**
2014/10/10	2.7	3	0.02	**50.96**	**0.85**	**0.74**	**0.90**	**0.86**
2014/10/13	2.6	2	0.02	**56.62**	**0.72**	0.30	**0.73**	**0.51**
2014/11/04	3.1	**19**	0.10	13.72	**0.96**	**0.72**	**0.94**	**0.73**

Note: d_{50} ($\times 10^5$ m), z_{ref} (mm), *FSE* (-) and k_r (kg/m^2/s^2) defined in Section 2.2. Simulated Nash–Sutcliffe and L_{NP} (Equation 13) efficiencies calculated for observed discharges >1 m^3/s, wrt, -H: discharge and -S: SSC.

$k_r = 0$ kg/m^2/s^2, that is, no raindrop erosion. The NASH-S performance of 5 February 2014 drops significantly from 0.415 to −0.020 when changing k_r from 0.02 to 0 kg/m^2/s^2. Subsequently, new simulations are run keeping the values of the other parameters but setting $FSE = 0$, that is, no shear stress erosion, for k_r-dominant events. The NASH-S score for event 5 February 2014 remains unchanged, while event 19 September 2014 the criteria slightly decrease: from 0.687 to 0.654 for NASH-S and from 0.699 to 0.681 for L_{NP}-S with respect to the results of the SA. For events 10 October 2014 and 13 October 2014, the NASH-S scores change from 0.742 to −0.099 (from 0.862 to 0.251 for L_{NP}-S) and from 0.298 to −0.005 (from 0.510 to −0.586 for L_{NP}-S), respectively. These results suggest that the simulations of 5 February 2014 and 19 September 2014 are actually raindrop erosion dominant whereas 10 October 2014 and 13 October 2014 are shear stress erosion dominant although their best simulation have a high k_r value. Simulations of events 5 February 2014 and 19 September 2014 are analysed in more detail below to confirm this assumption.

For event 5 February 2014, the discharge is underestimated to the extent that the simulated run-off does not generate enough shear stress to initiate sediment movement (Figure 2, *Q*). As a result, there is no shear stress erosion simulated. Therefore, NASH-S score for event 5 February 2014 remains constant when we set FSE to zero, as there is only simulated erosion by raindrop impact (Figure 2, *SSC*). As 5 February 2014 is a raindrop erosion event, d_{50} is not involved in the erosion simulation (Equations 9–12). Consequently, changing the d_{50} value has no impact on the SSC simulation for this event: in fact, running a simulation with a different d_{50} value only slightly changes the results for 5 February 2014. This may explain why the d_{50} value for the best 5 February 2014 simulation differs significantly from the other events (Table 6).

For event 19 September 2014, in terms of hydrodynamics, there is no underestimation of discharge (Figure 3, *Q*). However, there are three peaks of simulated SSC due to raindrop erosion whereas observations of discharge are lower than 0.5 m^3/s. Unfortunately, no observation of SSC is available during the first two peaks of simulated SSC.

Table 6 reveals that *FSE* and z_{ref} are either both high or both low, except for events 5 February 2014 and 19 September 2014, which break this pattern. This divergence might be linked to the correlation between *FSE* and z_{ref} when *FSE* is dominant factor: indeed, there is no shear stress erosion when the water depth is below z_{ref}, whatever the *FSE*. For k_r type events such as 5 February 2014 and 19 September 2014 the parameters *FSE* and z_{ref} governing shear stress erosion no longer have any impact, which explains why the same relationship is not found.

According to previous studies reviewed in Wicks and Bathurst (1996), the mean k_r coefficient varies around 30 J^{-1} for the soil textures present in the Claduègne catchment, mainly sandy loam (9.5% of the Claduègne catchment), loam (5.3%), silt loam (45.1%) and silt (17.1%), no k_r value is available for clay loam (22.9%). Here, the k_r values for k_r-dominant events are almost twice as high, which seems to indicate that the simulated raindrop erosion rate based on Equation (9) is underestimated.

Morgan (2001) provides guide values for the cohesion of the soil *COH* (kPa), based on those used in their model EUROSEM, but states that measured values, where available, should always be used in preference to the guideline values. There is no analytical formula that directly relates soil cohesion *COH* to the *FSE* parameter. However, the *COH* values given by Morgan (2001) are between 2 and 3 for 60% of the Claduègne catchment based on soil texture, that is, very low because *COH* can be as high as 10. It can therefore be concluded that the soil sensitivity to run-off erosion *FSE* is high in 60% of the catchment. However, Morgan et al. (1998) also emphasize that the relationship between soil cohesion and detachability of the soil by run-off is dependent upon the initial moisture content and structural conditions. These values are therefore only indicative as no unique relationship

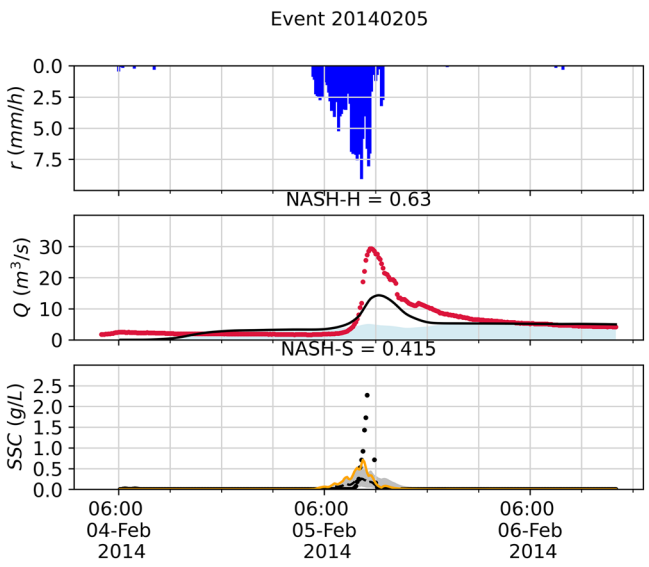

FIGURE 2 Hydrograph and sedigraph for event 5 February 2014. Rainfall rate (blue), observed discharge (red dots), simulated discharge (black), subsurface flow (light blue area), observed SSC (black dots), best SSC simulation (orange) and uncertainty interval from the sensitivity analysis (50% quantile in dashed black, 10% to 90% grey shaded area).

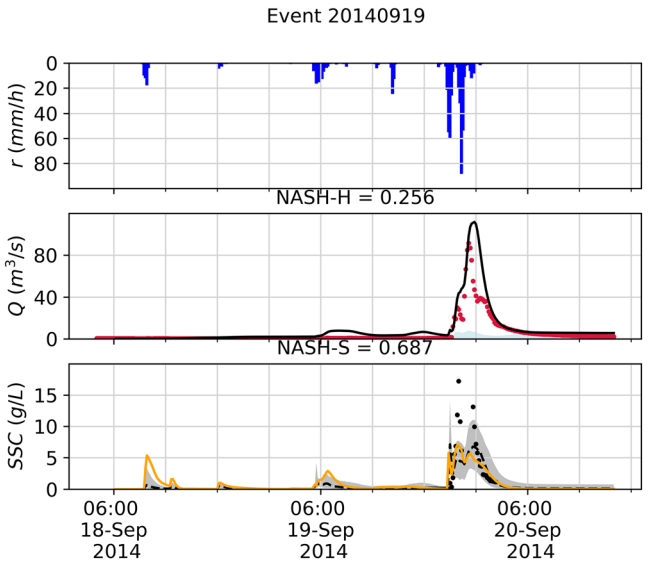

FIGURE 3 Hydrograph and sedigraph for event 19 September 2014. Rainfall rate (blue), observed discharge (red dots), simulated discharge (black), subsurface flow (light blue area), observed SSC (black dots), best SSC simulation (orange) and uncertainty interval from the sensitivity analysis (50% quantile in dashed black, 10% to 90% grey shaded area).

exists even for a single soil. It is therefore difficult to draw conclusions about the estimated *FSE* values, which can vary by an order of magnitude depending on the event, even if only the *FSE*-dominant events are considered.

In terms of grain size, the <20 µm fraction is found by Uber (2020) to be the dominant size class of the suspended sediment samples. She calculates that the ratio of the <20 µm fraction to the <63 µm fraction has a median of 0.78 for the 27 suspended sediment samples from the Claduègne where grain size distributions are measured. The d_{50}s estimated using the SA of the MARINE model range from 12 to 38 µm, which is in the same order of magnitude. This is not the case for event 5 February 2014, but d_{50} does not affect this simulation as explained before.

van Rijn (1984) assumes the reference level above the bed z_{ref} to be equal to the equivalent roughness heigh of Nikuradse k_h which can be approximated with $3d_{50}$. According to Tassi and Villaret (2014), from which the transport and shear stress erosion equations are derived, the reference level z_{ref} can be estimated as $z_{ref} = \max(k_h/2; 0.01\,\text{m})$. Here, the estimate of z_{ref} is close to the upper limit recommended by Tassi and Villaret (2014) suggesting that the best simulation tends to reduce shear stress erosion as it does not occur for $h < z_{ref}$.

Finally, taking into account the uncertainty associated in the simulation, both in the model structure and in the parameterisation, the analysis of the estimated parameter values helps to identify the weaknesses of the actual model and the possible paths for improvement.

3.2 | SA of vegetation cover factor *C*

This paragraph presents the results of the SA to *C* factor applying the method of Section 2.7. The obtained *C* values for MUSLE/RUSLE models for all the events and for the hillslope area are detailed in Table 7. The comparison does not consider cells representing the drainage network in MARINE because MUSLE and RUSLE are specifically designed for evaluating soil erosion at the field scale, not in drainage networks. Consequently, the RMSE (Equation 24) is solely calculated for the hillslope region at the resolution of the three models, which is 100 m × 100 m. This resolution is likely to have an impact on the results, which has not been tested in this study, as the values of the calibrated parameters (Table 6) of the MARINE model may depend on the resolution of the model.

The evaluation of the MARINE model's performance can be conducted by examining the consistency of the *C* values obtained through this comparative analysis with the range of *C* values derived from the Claduègne land cover. The *C* values should ideally fall within the following ranges, depending on the land cover type (Table 5 adapted from Panagos et al., 2015):

- from 0.0001 to 0.003 for forests and shrublands along slope (61% of the watershed),
- from 0.15 to 0.45 for vineyards, mainly situated in the southern area (16%),
- from 0.01 to 0.08 for natural grasslands (11%) and
- from 0.07 to 0.2 for cultivated fields (11%).

The calibrated *C* values for hillslopes are 0.0018 for MUSLE and 0.002 for RUSLE (Table 7). These values represent the weighted average *C* values for each model, taking into account the contribution of each event to the overall erosion.

Considering the lower and upper bound for each land-use category above, the area-weighted *C* factor for the Claduègne catchment may vary between 0.03 and 0.1. Then, the calibrated *C* values (Table 7) are underestimated by one order of magnitude with respect to this range of variation. This can be explained by the spatial distribution of erosion: Figure 4 shows that simulated erosion mainly occurs in cells close to the drainage network in the northern part and in the very southern part of the catchment. These zones correspond to steep hillslopes mainly covered by forest and shrublands where the *C* factors are lower than the average value calculated for the whole catchment. Indeed, the area-weighted value of *C* calculated only on cells showing erosion during all the events is 0.04. Overall, the average *C* value is close to the a priori value provided by the tabulated value as a function of land-use. This means that the MARINE computation is consistent with erosion estimations that MUSLE and RUSLE would have given while providing access to the temporal variability of erosion dynamics during the event.

4 | DISCUSSION

This section provides an overview of the advantages and limitations of the models tested. It is structured as follows: Section 4.1 describes

TABLE 7 Calibrated MUSLE and RUSLE *C* factor values, corresponding RMSE obtained through sensitivity analysis using MARINE results over hillslope area, ratio ErrC = $(C_{MUSLE} - C_{RUSLE})/C_{RUSLE}$ (%), initial soil moisture θ_i (median) (lowest: red, average: orange, highest: green).

Event	C_{MUSLE} ($\times 10^{-3}$)	$RMSE_{MUSLE}$ (t/ha)	C_{RUSLE} ($\times 10^{-3}$)	$RMSE_{RUSLE}$ (t/ha)	ErrC (%)	Median θ_i (%)
2011/11/04	4.66	5.7	2.73	7.6	70.9	59.2
2013/05/18	0.96	2.3	0.58	2.4	65.3	68.0
2013/10/20	2.39	2.3	0.58	2.8	312.0	58.6
2014/01/04	1.59	1.4	1.70	1.6	−6.2	73.5
2014/01/19	1.40	5.3	1.66	5.5	−15.7	73.7
2014/02/05	0.64	1.4	6.83	1.2	−90.7	71.8
2014/09/19	4.50	9.0	2.94	8.0	53.2	51.6
2014/10/10	0.39	1.1	0.79	1.0	−50.9	67.1
2014/10/13	0.19	0.6	0.42	0.6	−55.5	74.0
2014/11/04	2.03	7.1	1.82	9.2	11.6	65.1

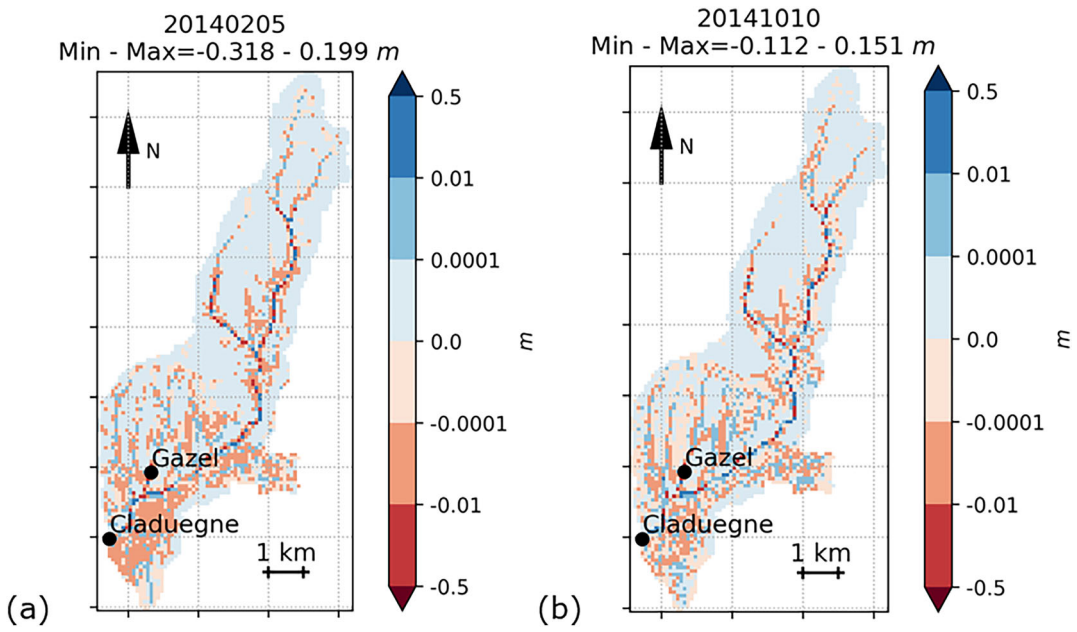

FIGURE 4 Map of erosion/deposition heights (m) with maximum height of erosion (Min) and deposition (Max) at the end of the event for (a) 5 February 2014 and (b) 10 October 2014.

the advances in our understanding of physical processes made possible by the results of simulations. Section 4.2 focuses on taking into account the spatial variability of the catchment characteristics in the simulations and its effect on the simulated erosion. Section 4.3 investigates the potential offered by access to the spatio-temporal variability of erosion dynamics provided by the distributed physically based model. Section 4.4 summarizes the limitations of the present study and possible improvements in the short and longer terms.

4.1 | Physical processes understanding

An advantage of the MARINE model is that it takes into account different physical processes of soil erosion, while empirical methods such as RUSLE and MUSLE do not. This can be helpful in gaining insight into the dynamics of the phenomenon and therefore in improving modelling. For example, simulations of suspended sediment transport with the MARINE model highlight a fundamental distinction between k_r or raindrop erosion type events and *FSE* or shear stress erosion type events. This categorization is investigated by running simulations with $k_r = 0$ kg/m^2/s^2 (no raindrop erosion) or $FSE = 0$ (no shear stress erosion). The results show that two events, 5 February 2014 and 19 September 2014, fall into the raindrop erosion type category, which cannot be simulated correctly with $k_r = 0$ kg/m^2/s^2. However, several other factors should be considered. In the case of 5 February 2014, the simulation underestimates the observed run-off and therefore possibly the shear stress, which could lead to compensation by raindrop erosion to correctly simulate the SSC at the outlet. Unfortunately, there are no in situ observations during floods that would allow us to distinguish the type of erosion that has occurred. However, with the democratization of LiDAR measurements taken before and after flood events, we can now have access to the spatial variability of the volumes eroded or deposited. This could help to confirm or refute the dynamics simulated by the MARINE model: Indeed, this spatial variability is also a function of the phenomenon causing the erosion. For instance, during high k_r events, where erosion zones are more extensive, the depths of eroded soil remain shallower.

As an advantage of physical modelling, MARINE also considers the influence of initial soil moisture on surface run-off erosion: Indeed, the infiltration rate, and therefore, the run-off height, depends on the initial soil moisture. MUSLE takes this into account through the run-off erosivity R_{MUSLE}, which is derived from the run-off volume simulated with MARINE (Equation 23). However, RUSLE does not take the initial soil moisture into account. As shown, when both RUSLE and MUSLE are calibrated using the MARINE results and aiming for the same range of eroded volumes, the C_{RUSLE} values are higher than C_{MUSLE} under wet conditions (4 January 2014, 19 January 2014, 5 February 2014, 10 October 2014 and 13 October 2014) and lower otherwise (Table 7). Events with a high initial saturation percentage have a higher run-off to rainfall ratio, leading to increased run-off and shear stress erosion in the MARINE simulations, which ultimately, via the run-off erosivity R_{MUSLE} of Equation (23), leads to higher erosion values in MUSLE. In addition, these events have lower rainfall erosivity R_{RUSLE} for RUSLE (Equation 16) compared with others (due to lower maximum local rainfall intensity, see Table 1). Consequently, larger C_{RUSLE} values are required to achieve comparable eroded volumes between MARINE and RUSLE. This is not the case for the 18 May 2013 event, although the initial soil moisture is also high for this event, most likely because the simulated run-off is underestimated and therefore the run-off.

4.2 | Spatial variability of erosion dynamics

The MARINE model takes into account the spatial variability of catchment characteristics, forcing and system states. In particular, the shape of the drainage network is represented synthetically. A main channel and overbanks with different roughness are considered. In contrast to

hillslopes where surface run-off is simulated in a continuous sheet, in the drainage network the water depths and flow velocities are higher and so is the shear stress. Shear stress erosion is therefore the dominant process simulated by the MARINE model in the drainage network.

Figure 5 illustrates this point by showing the differences between the simulated eroded volumes using the different models over all grid cells, over the drainage network cells only and over the hillslope cells only for the 18 May 2013 event. The spatial resolution of the grid is 100 m × 100 m for the three models. For the MARINE model, as it simulated both erosion and deposition processes, only the cells with simulated erosion at the end of the event are considered to calculate the eroded volume for each event. In the drainage network, MARINE simulates higher erosion. This discrepancy is due to the use of shear stress calculations based on channel cross sections rather than a flat cell. For hillslope erosion, the distribution of erosion is expected to be similar for the MUSLE and MARINE models, as MUSLE uses the run-off volume simulated by MARINE to calculate erosivity. However, notable differences emerge, especially for events with high k_r values (5 February 2014, 19 September 2014, 10 October 2014 and 13 October 2014). In fact, the dominant erosion-generating process in MARINE for these events is raindrop erosion, which is not directly represented in MUSLE, nor is it included in the run-off volume information transmitted from MARINE to MUSLE.

Although the parameters in the USLEs equation were originally designed to be applied globally over the whole catchment (Renard et al., 1997), it is possible to apply a USLE-type model in a distributed context. For example, the MARINE model incorporates the spatial variability of soil properties to simulate the surface run-off. Integrating the MARINE results into the R_{MUSLE} erosivity factor estimation introduces spatial variability into the MUSLE model results. This spatial variability of soil properties is currently absent from the RUSLE model and its inclusion may lead to a better understanding of the differences in C values estimated for the two models and potentially improve the results of the USLE-type model.

4.3 | Mapping of the erosion process

The SA of the C value in MUSLE and RUSLE using the MARINE model as a reference resulted in C values close to the range of variation estimated directly from the land cover map of the Claduègne catchment. The MARINE SSC simulations are therefore consistent with RUSLE and MUSLE erosion estimates, while providing access to the spatio-temporal variability of erosion dynamics during the event, which is not possible with USLE-type models.

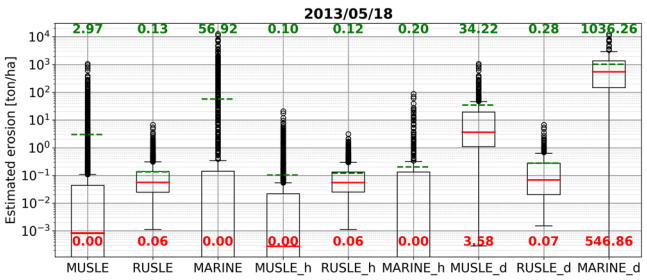

FIGURE 5 Estimated erosion (t/ha) for the 18 May 2013 event using MUSLE, RUSLE and MARINE models with a resolution of 100 m ×100 m over all grid cells, over the hillslope cells only (_h) and over the drainage network cells only (_d) using calibrated C factor values for MUSLE and RUSLE (Table 7), area statistics: median (red), mean (green).

Consequently, one of the results of this study is the mapping of areas subject to erosion and deposition hazards during events or during a series of events. In order to put this understanding of erosion dynamics into practice, it would be very useful to produce a hazard map illustrating areas at risk of erosion and deposition. Such a map could be a valuable tool for environmental decision-makers and planners. In our study, the erosion pattern in the MARINE framework can be explored for different event types (shear stress and raindrop erosion). For each event, each cell is identified as an erosion cell (−1) or a deposition cell (+1) depending on its situation at the end of the event. These binary maps are then summed for all the events according to their type (two raindrop erosion dominant events, 5 February 2014 and 19 September 2014, and eight shear stress erosion dominant events). Any cell with a negative value is considered as a cell with predominant erosion over all the events of a given type (in red on Figure 6), any cell with a positive value is considered as a cell with predominant deposition (in blue on Figure 6). The map of erosion zones is then overlaid on the slope map to analyse erosion patterns according to event type (shear stress or raindrop erosion dominant, Figure 6). For shear stress erosion events, erosion occurs mainly along the main flow path when the gradient of the slope gradient is high (Figure 6b). For raindrop events, erosion also occurs in hillslope, with a larger surface area affected (Figure 6a). Of course, it is difficult to generalize these conclusions as only two of the events studied are raindrop erosion dominant, but this approach is a statistical method that helps to visualize and understand erosion risk patterns in order to consider effective soil conservation and land management strategies.

4.4 | Improvements and future work

Some key factors that can improve our understanding of the erosion dynamics in our study need to be considered in the next steps.

As mentioned above, the coefficients FSE, k_r, C and K are assumed to be uniform across the entire catchment and this choice certainly has an impact on the simulation results. The next stage is to identify the location of potential sediment sources and particularly Badlands, as Uber et al. (2021) have done on the Claduègne catchment, and to study how this information can be effectively incorporated into the models, targeting the parameters of soil sensitivity to erosion.

For future research, it would be worth exploring alternative indices in the calculation of the rainfall erosivity factor R_{RUSLE} that take into account the duration of rainfall exceeding certain intensities within an event, in order to better represent the most intense rainfall periods.

Land cover and land-use can change over time, and these factors can have a significant impact on erosion rates, which is not considered in this study. Future research could take into account the dynamic nature of these variables to provide a more accurate representation of erosion processes in the catchment. Bircher et al. (2019) also highlight the importance of the spatial resolution of the DEM in calculating the topographical LS factor and predicting soil erosion risk. For future applications, the use of fine resolution DEMs is recommended to improve the accuracy of the LS factor calculation.

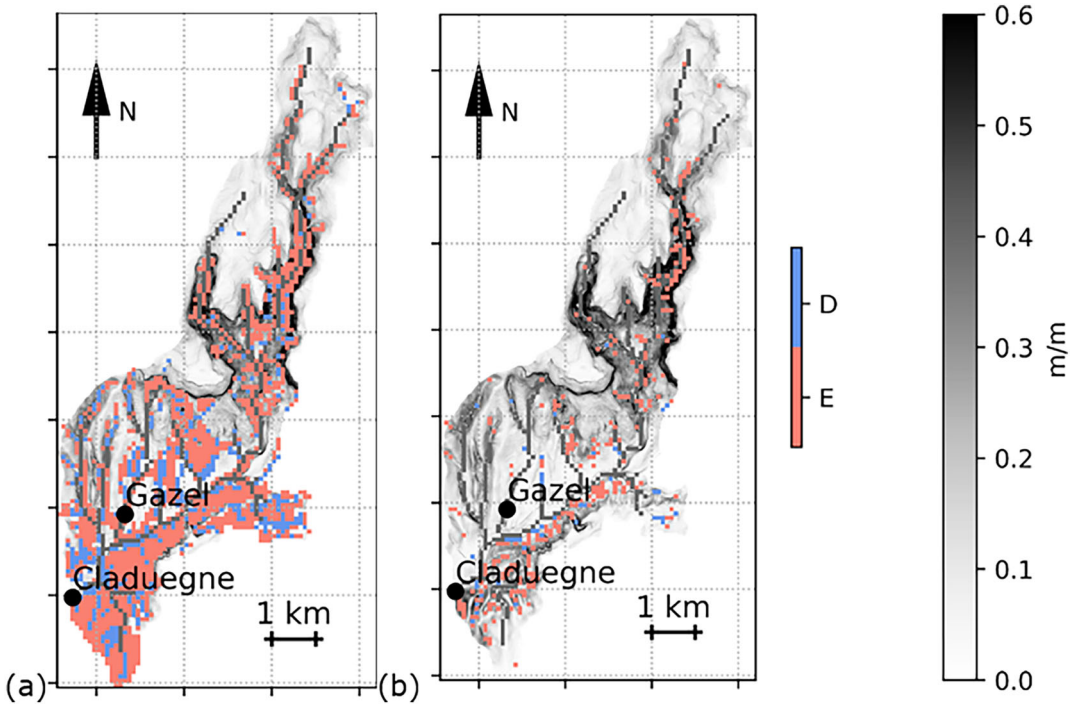

FIGURE 6 Cumulative binary erosion/deposition map over slope map (m/m) for (a) raindrop erosion dominant (5 February 2014 and 19 September 2014) and (b) shear stress erosion dominant events, erosion cells are highlighted in red, deposition cells in blue and drainage network cells in grey.

One of the advantages of the erosion maps produced by the distributed model is that they can be used to produce maps of areas at risk of erosion by cross-referencing them with maps of vulnerability, including areas with infrastructure or areas of ecological concern such as spawning grounds. This will facilitate the identification of areas where erosion and/or deposition pose a significant risk to infrastructure or ecology. However, these erosion maps and their spatial variability have not been validated yet as part of this study. LiDAR measurements taken before and after flood events, which provide access to the spatial variability of the volumes eroded or deposited, will be used to confirm or refute the dynamics simulated by the MARINE model. Although few measurements of this type are currently available, they will provide valuable information for identifying the dynamics correctly simulated by the model and the need for improvement.

5 | CONCLUSIONS

In this study, we evaluate the performance of using a spatially distributed, physically based model to estimate erosion in the Claduègne catchment during flash floods. The aim is to assess how the use of a physically based model affects the efficiency of erosion estimation during flash floods compared with widely used models in erosion estimation such as RUSLE and MUSLE.

A physically based hydrological model designed for flash floods, the MARINE model, is used for this purpose. MARINE takes advantage of distributed data to simulate the hydrodynamic response of the catchment and suspended sediment transport. The results of the MARINE simulations show a significant distinction between k_r or raindrop-type and *FSE* or shear stress-type events in the MARINE simulations. Furthermore, the analysis of the results highlights the need for further investigation to improve the modelling of raindrop erosion within MARINE.

A SA is then performed to estimate the cover-management factor *C* that results in the lowest RMSE between erosion volumes (t/ha) simulated by MUSLE/RUSLE and MARINE for each flash flood event. The estimated *C* values are close to the range of variation estimated directly from the land cover map of the Claduègne catchment. The special cases were analysed and logically linked to the particularities of the different models: erosion on flat cells, whether initial moisture was taken into account or not, run-off overestimated or underestimated by the MARINE model. This allowed us to better identify the limitations of the USLE-type models and also to define ways to improve the modelling of suspended transport in the MARINE model.

Finally, the strengths of a physically based distributed model were highlighted: understanding of processes, access to the variability of spatio-temporal erosion dynamics, production of a hazard map which, in combination with a vulnerability map, can be useful to environmental decision-makers and planners in identifying areas at risk from erosion and deposition hazards. Of course, this will require validation of the simulated spatial variability of erosion, which remains to be done, but for which a number of avenues have been suggested.

AUTHOR CONTRIBUTIONS

Atiyeh Hosseinzadeh contributed to methodology, performing simulations and post-processing and writing. Hélène Roux contributed to conceptualization, funding acquisition, methodology, data collection, software provision and development, supervision and writing. Ludovic Cassan contributed to conceptualization, funding acquisition, methodology, software development, supervision and writing. Audrey Douinot contributed to methodology, performing simulations, data collection and software development.

ACKNOWLEDGEMENTS

This work has been funded by Office Français de la Biodiversité and Région Occitanie Pyrénées-Méditerranée under Allocation No. 20007302/ALDOCT-000988. This work was granted access to the data of Claduègne catchment thanks to Observatoire Hydro-météorologique Méditerranéen Cévennes-Vivarais and more specifically Guillaume Nord and Brice Boudevillain, whom the authors would like to thank.

CONFLICT OF INTEREST STATEMENT

The authors declare that they have no known competing financial interests or personal relationships that could have appeared to influence the work reported in this paper.

DATA AVAILABILITY STATEMENT

All the data concerning the Claduègne catchment are available thanks to the data paper of Nord et al. (2017), https://doi.org/10.5194/essd-9-221-2017.

ORCID

Hélène Roux https://orcid.org/0000-0001-7076-5015

REFERENCES

Aksoy, H. & Kavvas, M.L. (2005) A review of hillslope and watershed scale erosion and sediment transport models. *Catena*, 64(2–3), 247–271. Available from: https://doi.org/10.1016/j.catena.2005.08.008

Alewell, C., Borrelli, P., Meusburger, K. & Panagos, P. (2019) Using the USLE: chances, challenges and limitations of soil erosion modelling. *International Soil and Water Conservation Research*, 7(3), 203–225. Available from: https://doi.org/10.1016/j.iswcr.2019.05.004

Bannari, A., Kadhem, G., El-Battay, A., Hameid, N.A. & Rouai, M. (2016) Assessment of land erosion and sediment accumulation caused by runoff after a flash-flooding storm using topographic profiles and spectral indices. *Advances in Remote Sensing*, 5(4), 315–354. Available from: https://doi.org/10.4236/ars.2016.54024

Beven, K. (1989) Changing ideas in hydrology—the case of physically-based models. *Journal of Hydrology*, 105(1–2), 157–172. Available from: https://doi.org/10.1016/0022-1694(89)90101-7

Bircher, P., Liniger, H.P. & Prasuhn, V. (2019) Comparing different multiple flow algorithms to calculate RUSLE factors of slope length (L) and slope steepness (S) in Switzerland. *Geomorphology*, 346, 106850. Available from: https://doi.org/10.1016/j.geomorph.2019.106850

Borga, M., Stoffel, M., Marchi, L., Marra, F. & Jakob, M. (2014) Hydrogeomorphic response to extreme rainfall in headwater systems: flash floods and debris flows. *Journal of Hydrology*, 518, 194–205. Available from: https://doi.org/10.1016/j.jhydrol.2014.05.022

Borrelli, P., Alewell, C., Alvarez, P., Anache, J.A.A., Baartman, J., Ballabio, C., et al. (2021) Soil erosion modelling: a global review and statistical analysis. *Science of the Total Environment*, 780, 146494. Available from: https://doi.org/10.1016/j.scitotenv.2021.146494

Branger, F. & Thollet, F. (2016) *Documentation Base de Données des Observatoires en Hydrologie (BDOH)* Technical report. INRAE.

Braud, I., Ayral, P.A., Bouvier, C., Branger, F., Delrieu, G., Le Coz, J., et al. (2014) Multi-scale hydrometeorological observation and modelling for flash flood understanding. *Hydrology and Earth System Sciences*, 18(9), 3733–3761. Available from: https://doi.org/10.5194/hess-18-3733-2014

Cea, L., Legout, C., Grangeon, T. & Nord, G. (2016) Impact of model simplifications on soil erosion predictions: application of the GLUE methodology to a distributed event-based model at the hillslope scale. *Hydrological Processes*, 30(7), 1096–1113. Available from: https://doi.org/10.1002/hyp.10697

David, A., Bancon-Montigny, C., Salles, C., Rodier, C. & Tournoud, M.G. (2012) Contamination of riverbed sediments by hazardous substances in the Mediterranean context: influence of hydrological conditions. *Journal of Hydrology*, 468, 76–84. Available from: https://doi.org/10.1016/j.jhydrol.2012.08.015

De Roo, A.P.J., Offermans, R.J.E. & Cremers, N.H.D.T. (1996) LISEM: a single-event, physically based hydrological and soil erosion model for drainage basins. II: sensitivity analysis, validation and application. *Hydrological Processes*, 10(8), 1119–1126. Available from: https://doi.org/10.1002/(SICI)1099-1085(199608)10:8%3C1119::AID-HYP416%3E3.0.CO;2-V

Desmet, P.J.J. & Govers, G. (1996) A GIS procedure for automatically calculating the USLE LS factor on topographically complex landscape units. *Journal of Soil and Water Conservation*, 51(5), 427–433.

Djoukbala, O., Hasbaia, M., Benselama, O. & Mazour, M. (2019) Comparison of the erosion prediction models from USLE, MUSLE and RUSLE in a Mediterranean watershed, case of Wadi Gazouana (NW of Algeria). *Modeling Earth Systems and Environment*, 5(2), 725–743. Available from: https://doi.org/10.1007/s40808-018-0562-6

Dunkerley, D.L. (2019) Rainfall intensity bursts and the erosion of soils: an analysis highlighting the need for high temporal resolution rainfall data for research under current and future climates. *Earth Surface Dynamics*, 7(2), 345–360. Available from: https://doi.org/10.5194/esurf-7-345-2019

Eeckman, J., Roux, H., Douinot, A., Bonan, B. & Albergel, C. (2021) A multi-sourced assessment of the spatiotemporal dynamics of soil moisture in the MARINE flash flood model. *Hydrology and Earth System Sciences*, 25(3), 1425–1446. Available from: https://doi.org/10.5194/hess-25-1425-2021

Fortugno, D., Boix-Fayos, C., Bombino, G., Denisi, P., Quinonero Rubio, J.M., Tamburino, V., et al. (2017) Adjustments in channel morphology due to land-use changes and check dam installation in mountain torrents of Calabria (southern Italy). *Earth Surface Processes and Landforms*, 42(14), 2469–2483. Available from: https://doi.org/10.1002/esp.4197

Garambois, P.A., Roux, H., Larnier, K., Labat, D. & Dartus, D. (2015a) Parameter regionalization for a process-oriented distributed model dedicated to flash floods. *Journal of Hydrology*, 525, 383–399. Available from: https://doi.org/10.1016/j.jhydrol.2015.03.052

Garambois, P.A., Roux, H., Larnier, K., Labat, D. & Dartus, D. (2015b) Characterization of catchment behaviour and rainfall selection for flash flood hydrological model calibration: catchments of the eastern Pyrenees. *Hydrological Sciences Journal*, 60(3), 424–447. Available from: https://doi.org/10.1080/02626667.2014.909596

Gaume, E., Bain, V., Bernardara, P., Newinger, O., Barbuc, M., Bateman, A., et al. (2009) A compilation of data on European flash floods. *Journal of Hydrology*, 367(1–2), 70–78. Available from: https://doi.org/10.1201/9780203883020.ch186

González-Hidalgo, J.C., Peña-Monné, J.L. & de Luis, M. (2007) A review of daily soil erosion in Western Mediterranean areas. *Catena*, 71(2), 193–199. Available from: https://doi.org/10.1016/j.catena.2007.03.005

Gwapedza, D., Hughes, D.A. & Slaughter, A.R. (2018) Spatial scale dependency issues in the application of the Modified Universal Soil Loss Equation (MUSLE). *Hydrological Sciences Journal*, 63(13–14), 1890–1900. Available from: https://doi.org/10.1080/02626667.2018.1546388

Habets, F., Boone, A., Champeaux, J.L., Etchevers, P., Franchisteguy, L., Leblois, E., et al. (2008) The SAFRAN-ISBA-MODCOU hydrometeorological model applied over France. *Journal of Geophysical Research: Atmospheres*, 113(D6), Available from: https://doi.org/10.1029/2007JD008548

Hosseinzadeh, A., Roux, H., Cassan, L. & Douinot, A. (2022) Application of GSA/GLUE methods to evaluate the representation of suspended sediment transport during flash floods in a rainfall-runoff model. *IFAC-PapersOnLine*, 55(5), 90–95. Available from: https://doi.org/10.1016/j.ifacol.2022.07.645

Huynh, N.N.T., Garambois, P.A., Colleoni, F. & Javelle, P. (2023) Signatures-and-sensitivity-based multi-criteria variational calibration for distributed hydrological modeling applied to Mediterranean floods. *Journal of Hydrology*, 625, 129992. Available from: https://doi.org/10.1016/j.jhydrol.2023.129992

Kaffas, K., Papaioannou, G., Varlas, G., Al Sayah, M.J., Papadopoulos, A., Dimitriou, E., et al. (2022) Forecasting soil erosion and sediment yields during flash floods: the disastrous case of Mandra, Greece, 2017. *Earth Surface Processes and Landforms*, 47(7), 1744–1760. Available from: https://doi.org/10.1002/esp.5344

Kinnell, P.I.A., Wang, J. & Zheng, F. (2018) Comparison of the abilities of WEPP and the USLE-M to predict event soil loss on steep loessal slopes in China. *Catena*, 171, 99–106. Available from: https://doi.org/10.1016/j.catena.2018.07.007

Laflen, J.M., Lane, L.J. & Foster, G.R. (1991) WEPP: a new generation of erosion prediction technology. *Journal of Soil and Water Conservation*, 46(1), 34–38.

Laws, J.O. & Parsons, D.A. (1943) The relation of raindrop-size to intensity. *Eos, Transactions American Geophysical Union*, 24(2), 452–460. Available from: https://doi.org/10.1029/TR024i002p00452

Le Coz, J., Renard, B., Bonnifait, L., Branger, F., & Le Boursicaud, R. (2014) Combining hydraulic knowledge and uncertain gaugings in the estimation of hydrometric rating curves: A Bayesian approach. *Journal of Hydrology*, 509, 573–587. https://doi.org/10.1016/j.jhydrol.2013.11.016

León, V.M., Moreno-González, R., García, V. & Campillo, J.A. (2017) Impact of flash flood events on the distribution of organic pollutants in surface sediments from a Mediterranean coastal lagoon (Mar Menor, SE Spain). *Environmental Science and Pollution Research*, 24(5), 4284–4300. Available from: https://doi.org/10.1007/s11356-015-4628-y

McCool, D.K., Brown, L.C., Foster, G.R., Mutchler, C.K. & Meyer, L.D. (1987) Revised slope steepness factor for the Universal Soil Loss Equation. *Transactions of ASAE*, 30(5), 1387–1396. Available from: https://doi.org/10.13031/2013.30576

Morgan, R.P.C. (2001) A simple approach to soil loss prediction: a revised Morgan–Morgan–Finney model. *Catena*, 44(4), 305–322. Available from: https://doi.org/10.1016/S0341-8162(00)00171-5

Morgan, R.P.C., Morgan, D.D.V. & Finney, H.J. (1984) A predictive model for the assessment of soil erosion risk. *Journal of Agricultural Engineering Research*, 30, 245–253. Available from: https://doi.org/10.1016/S0021-8634(84)80025-6

Morgan, R.P.C., Quinton, J.N., Smith, R.E., Govers, G., Poesen, J.W.A., Chisci, G., et al. (1998) The EUROSEM model. In: *Modelling soil erosion by water*. Berlin, Heidelberg: Springer, pp. 389–398 https://doi.org/10.1007/978-3-642-58913-3_29

Nearing, M.A., Wei, H., Stone, J.J., Pierson, F.B., Spaeth, K.E., Weltz, M.A., et al. (2011) A rangeland hydrology and erosion model. *Transactions of the ASABE*, 54(3), 901–908. Available from: https://doi.org/10.13031/2013.37115

Nguyen, P., Thorstensen, A., Sorooshian, S., Hsu, K., AghaKouchak, A., Sanders, B., et al. (2016) A high resolution coupled hydrologic–hydraulic model (HiResFlood-UCI) for flash flood modeling. *Journal of Hydrology*, 541, 401–420. Available from: https://doi.org/10.1016/j.jhydrol.2015.10.047

Nord, G., Boudevillain, B., Berne, A., Branger, F., Braud, I., Dramais, G., et al. (2017) A high space–time resolution dataset linking meteorological forcing and hydro-sedimentary response in a mesoscale Mediterranean catchment (Auzon) of the Ardèche region, France. *Earth System Science Data*, 9(1), 221–249. Available from: https://doi.org/10.5194/essd-9-221-2017

OHMCV Observatory—Ozcar-Ri. (n.d.) Retrieved 19 July 2023, from https://www.ozcar-ri.org/ohmcv-observatory/

Panagos, P., Borrelli, P., Meusburger, K., Alewell, C., Lugato, E. & Montanarella, L. (2015) Estimating the soil erosion cover-management factor at the European scale. *Land Use Policy*, 48, 38–50. Available from: https://doi.org/10.1016/j.landusepol.2015.05.021

Papanicolaou, A.T.N., Elhakeem, M., Krallis, G., Prakash, S. & Edinger, J. (2008) Sediment transport modeling review—current and future developments. *Journal of Hydraulic Engineering*, 134(1), 1–14. Available from: https://doi.org/10.1061/(ASCE)0733-9429(2008)134:1(1)

Renard, K.G., Foster, G.R., Weesies, G.A., McCool, D.K. & Yoder, D.C. (1997) *Predicting soil erosion by water: a guide to conservation planning with the Revised Universal Soil Loss Equation (RUSLE)*. U.S. Department of Agriculture Agriculture Handbook No. 703, 404 pp.

Roux, H., Labat, D., Garambois, P.A., Maubourguet, M.M., Chorda, J. & Dartus, D. (2011) A physically-based parsimonious hydrological model for flash floods in Mediterranean catchments. *Natural Hazards and Earth System Sciences*, 11(9), 2567–2582. Available from: https://doi.org/10.5194/nhess-11-2567-2011

Sadaoui, M., Ludwig, W., Bourrin, F. & Raimbault, P. (2016) Controls, budgets and variability of riverine sediment fluxes to the Gulf of Lions (NW Mediterranean Sea). *Journal of Hydrology*, 540, 1002–1015. Available from: https://doi.org/10.1016/j.jhydrol.2016.07.012

Sadeghi, S.H.R., Gholami, L., Khaledi Darvishan, A. & Saeidi, P. (2014) A review of the application of the MUSLE model worldwide. *Hydrological Sciences Journal*, 59(2), 365–375. Available from: https://doi.org/10.1080/02626667.2013.866239

Schmidt, S., Tresch, S. & Meusburger, K. (2019) Modification of the RUSLE slope length and steepness factor (LS-factor) based on rainfall experiments at steep alpine grasslands. *MethodsX*, 6, 219–229. Available from: https://doi.org/10.1016/j.mex.2019.01.004

Sieber, A. & Uhlenbrook, S. (2005) Sensitivity analyses of a distributed catchment model to verify the model structure. *Journal of Hydrology*, 310(1–4), 216–235. Available from: https://doi.org/10.1016/j.jhydrol.2005.01.004

Stefanidis, S., Alexandridis, V. & Ghosal, K. (2022) Assessment of water-induced soil erosion as a threat to Natura 2000 protected areas in Crete Island, Greece. *Sustainability*, 14(5), 2738. Available from: https://doi.org/10.3390/su14052738

Tassi, P. & Villaret, C. (2014) *Sisyphe v6.3 user's manual*. Chatou, France: Recherche et développement, Électricité de France.

Uber, M. (2020) *Suspended sediment production and transfer in mesoscale catchments: a new approach combining flux monitoring, fingerprinting and distributed numerical modeling*. Doctoral dissertation. Grenoble, France: Université Grenoble Alpes.

Uber, M., Nord, G., Legout, C. & Cea, L. (2021) How do modeling choices and erosion zone locations impact the representation of connectivity and the dynamics of suspended sediments in a multi-source soil erosion model? *Earth Surface Dynamics*, 9(1), 123–144. Available from: https://doi.org/10.5194/esurf-9-123-2021

USGS by Kansas Water Science Center. (2005) Flood definitions. Retrieved 19 July 2023, from https://www.usgs.gov/media/files/flood-definitions

van Rijn, L.C. (1984) Sediment transport, part I: bed load transport. *Journal of Hydraulic Engineering*, 110(10), 1431–1456. Available from: https://doi.org/10.1061/(ASCE)0733-9429(1984)110:10(1431)

Viollet, P.L., Chabard, J.P., & Esposito, P. (2003). Mécanique des fluides appliquée: écoulements incompressibles dans les circuits, canaux et rivières, autour des structures et dans l'environnement. Presses des Ponts.

Wicks, J.M. & Bathurst, J.C. (1996) SHESED: a physically based, distributed erosion and sediment yield component for the SHE hydrological modelling system. *Journal of Hydrology*, 175(1–4), 213–238. Available from: https://doi.org/10.1016/S0022-1694(96)80012-6

Williams, J.R. (1975) Sediment routing for agricultural watersheds. *JAWRA Journal of the American Water Resources Association*, 11(5), 965–974. Available from: https://doi.org/10.1111/j.1752-1688.1975.tb01817.x

Wischmeier, W.H. & Smith, D.D. (1978) *Predicting rainfall erosion losses: a guide to conservation planning*, Vol. The USDA Agricultural Handbook No. 537. Beltsville, Maryland: Department of Agriculture, Science and Education Administration.

How to cite this article: Hosseinzadeh, A., Roux, H., Cassan, L. & Douinot, A. (2024) Combined use of physically based hydrological model and empirical models to improve parameterisation of erosion processes in a flash flood prone catchment. *Earth Surface Processes and Landforms*, 1–15. Available from: https://doi.org/10.1002/esp.5946